energies

MDPI

Article

Effects of Ball Milling and TiF_3 Addition on the Dehydrogenation Temperature of $Ca(BH_4)_2$ Polymorphs

Isabel Llamas Jansa [1,*], Oliver Friedrichs [2], Maximilian Fichtner [3], Elisa Gil Bardají [4], Andreas Züttel [5] and Bjørn C. Hauback [1]

1 Institute for Energy Technology, Box 40, 2027 Kjeller, Norway; Bjorn.Hauback@ife.no
2 Empa Mat. Sci. & Technol., Uberlandstr. 129, CH-8600 Dubendorf, Switzerland; veroil@web.de
3 Helmholtz Institute Ulm, Helmholtzstraβe 11, 89081 Ulm, Germany; maximilian.fichtner@kit.edu
4 Karlsruhe Institute of Technology, POB 3640, D-76021 Karlsruhe, Germany; elisa.gil@kit.edu
5 École Polytechnique Fédérale de Lausanne Valais/Wallis, Laboratory of Materials for Renewable Energy, Institute of Chemical Sciences and Engineering and Basic Science Faculty, Energypolis, Rue de l'Industrie 17, CH-1950 Sion, Switzerland; andreas.zuettel@epfl.ch
* Correspondence: isabel.llamas@ife.no

Received: 19 August 2020; Accepted: 10 September 2020; Published: 15 September 2020

Abstract: The changes introduced by both ball milling and the addition of small amounts of TiF_3 in the kinetics of the hydrogen desorption of three different $Ca(BH_4)_2$ polymorphs (α, β and γ) have been systematically investigated. The samples with different polymorphic contents, before and after the addition of TiF_3, were characterized by powder X-ray diffraction and vibrational spectroscopy. The hydrogen desorption reaction pathways were monitored by differential scanning calorimetry. The hydrogen desorption of $Ca(BH_4)_2$ depends strongly on the amount of coexistent α, β and γ polymorphs as well as additional ball milling and added TiF_3 to the sample. The addition of TiF_3 increased the hydrogen desorption rate without significant dissociation of the fluoride. The combination of an α-$Ca(BH_4)_2$ rich sample with 10 mol% of TiF_3 and 8 h of milling led to up to 27 °C decrease of the hydrogen desorption peak temperature.

Keywords: calcium borohydride; hydrogen storage; powder X-ray diffraction; ball milling; additives; kinetics of the hydrogen desorption; polymorphs; vibrational spectroscopy; reaction pathways; differential scanning calorimetry

1. Introduction

The alkali earth metal calcium borohydride, $Ca(BH_4)_2$, possesses 11.6 wt.% gravimetric and 130 kgm^{-3} volumetric hydrogen densities, respectively, and therefore it is often considered an attractive hydrogen storage system either alone or in composites [1–7]. Moreover, its calculated low reaction enthalpy, 32 $kJmol^{-1}H_2$ for equation

$$3Ca(BH_4)_2 \rightarrow CaB_6 + 2CaH_2 + 10H_2, \quad (1)$$

that leads to a 9.6 wt.% H_2 yield [8–12] and its possible reversibility at moderate conditions [2,13–16], make $Ca(BH_4)_2$ a particularly attractive hydrogen storage candidate.

However, this is a complicated borohydride to control. There are four known polymorphs of $Ca(BH_4)_2$. Three of them are referred to as low-temperature phases, α-, α'-, and γ-$Ca(BH_4)_2$, while only one high-temperature modification, β-$Ca(BH_4)_2$, has been identified [1,10,17].

Their crystal structures have been assigned to orthorhombic space groups in the cases of α- (*Fddd* [8,18] or *F2dd* [17]) and γ-$Ca(BH_4)_2$ (*Pbca* [18]), and to tetragonal space groups for α'- (*I-42d* [17]) and β-$Ca(BH_4)_2$ ($P4_2/m$ [19] or *P-4* [17]). Most transitions between the polymorphs are of first-order [20], with the α-α' transition being of second order [17]. Because of the small enthalpy differences between the various polymorphs ($\Delta H(\alpha\text{-}\beta)$ = 13.03 $kJmol^{-1}H_2$, $\Delta H(\alpha\text{-}\gamma)$ = 6.08 $kJmol^{-1}H_2$ [19]; or $\Delta H(\alpha\text{-}\beta)$ = 8.59 $kJmol^{-1}H_2$, $\Delta H(\alpha\text{-}\gamma)$ = 3.38 $kJmol^{-1}H_2$ [20]), it is common that they appear mixed in different ratios in batches produced by the same synthesis method. This fact complicates the characterization of the thermodynamics and kinetics of $Ca(BH_4)_2$ and the future reproducibility for practical applications [1].

The complete dehydrogenation of $Ca(BH_4)_2$ takes place between room temperature (RT) and 600 °C [1,10,21]. The process leads to three main endothermic events that can be assigned to the reversible α to β, low-temperature-to-high-temperature polymorphic transformation (between 160 and 250 °C), the decomposition of the high- temperature polymorph β (above 350 °C), and the decomposition of intermediates formed from metastable phases (CaB_2H_x has been proposed [22]). The temperatures at which these events occur depend strongly on experimental conditions such as type of gas flow, heating rate, et cetera, but also on the partial content of the different $Ca(BH_4)_2$ polymorphs in the sample [1]. In particular, our previous detailed study of the role of $Ca(BH_4)_2$ polymorphs showed increases of the decomposition temperature of up to 15 °C in samples containing γ-$Ca(BH_4)_2$ compared to a purer α-$Ca(BH_4)_2$, and of about 6 °C lower decomposition temperatures for a pure β- $Ca(BH_4)_2$ sample synthesized by a solvent free method compared to the high-temperature β modification obtained via the polymorphic transformation of α-$Ca(BH_4)_2$. The polymorphic content was also found to affect the amount of hydrogen released in each of the decomposition steps, with an increase of the mass loss for samples containing more of the α-$Ca(BH_4)_2$ polymorph [1]. These results confirm that the pure $Ca(BH_4)_2$ polymorphs have different kinetic barriers and that the polymorphic content of a sample determines the decomposition kinetics [1].

On the other hand, it is known that the decomposition temperature of $Ca(BH_4)_2$ is decreased both by ball milling and by the addition of additives in small amounts [2,15,21]. Recently, similar effects have been observed in other light metal borohydrides such as $NaBH_4$ [23–26] and $Mg(BH_4)_2$ [27–29], and on reactive composites like the $Ca(BH_4)_2$-MgH_2 system [6]. Moreover, fluoride additives such as TiF_3 and NbF_5 not only have shown that the reversibility of $Ca(BH_4)_2$ is possible under moderate conditions (140 bar and near RT), but also that they significantly decrease the decomposition temperature of the borohydride when compared to chlorides [14,15,27,30]. However, the mechanisms by which the improvement happens are not yet known.

Based on these previous works, we present here a study on the effects on the dehydrogenation temperature of the three most common polymorphs of $Ca(BH_4)_2$, α, β and γ, by both ball milling and the addition of small amounts of TiF_3.

2. Results and Discussion

2.1. Milling Effects on As-Received $Ca(BH_4)_2$

Before analyzing the influence of TiF_3 on the decomposition properties of $Ca(BH_4)_2$ polymorphs, the effects of ball milling on the as-received $\alpha_{\beta\gamma}$- and γ-$Ca(BH_4)_2$ were studied (Table 1 and Figure 1). Due to the lack of enough original material these milling experiments were not performed on pure β-$Ca(BH_4)_2$.

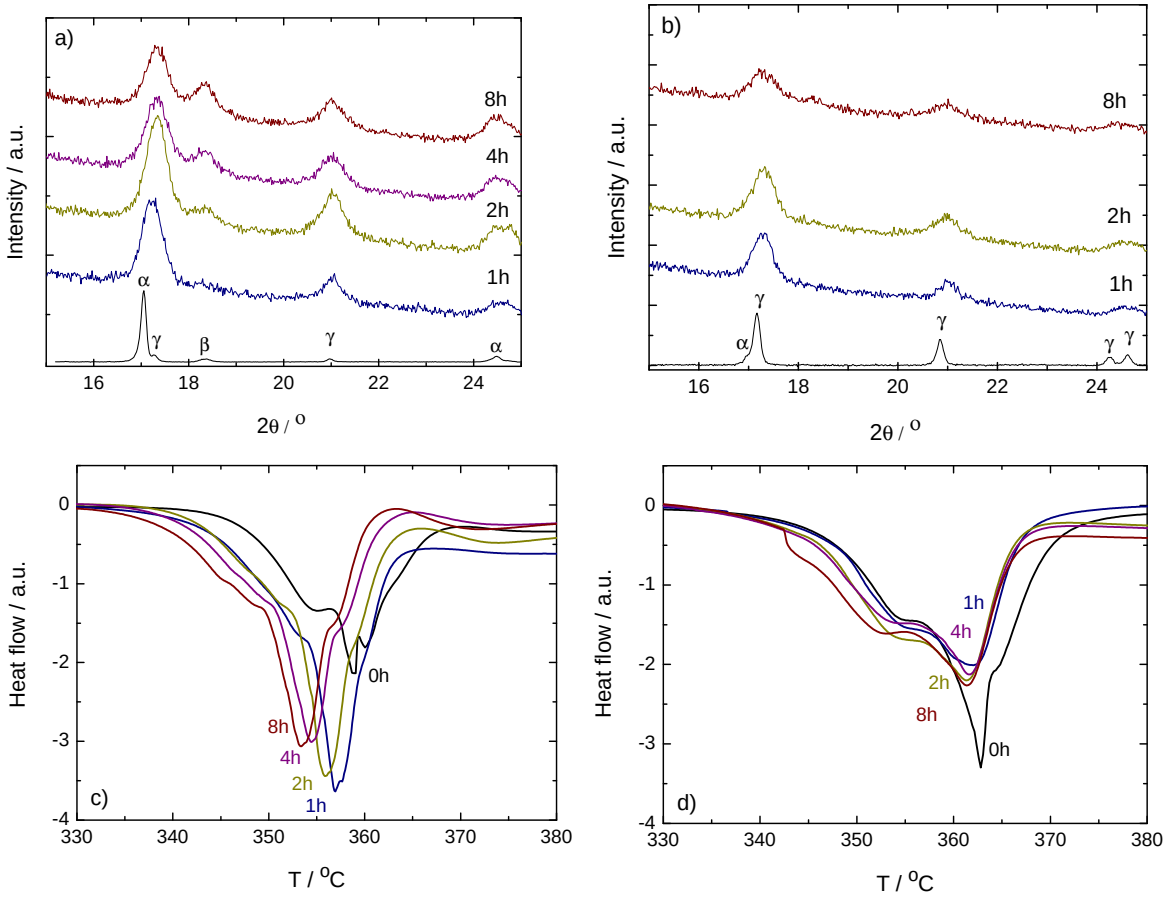

Figure 1. Top: Powder X-ray diffraction (PXD) results on ball milled $\alpha_{\beta\gamma}$ (left-hand side, (**a**)) and γ (right-hand side, (**b**)). Samples were taken from the vials after 1, 2, 4 and 8 h milling. The pattern of the as-received sample is included for comparison. Missing 4 h curve in the γ case due to low signal-to-noise-ratio. Below: Corresponding differential scanning calorimetry (DSC) curves of ball milled $\alpha_{\beta\gamma}$ (left-hand side, (**c**)) and γ (right-hand side, (**d**)). Only the main decomposition region between 330 and 380 °C is shown. Measurements were done under dynamic conditions in protective Ar flow, with 2 °C/min heating rates. The curves have been shifted in the vertical axis to show the peak trend.

In addition to the broadening of the diffraction peaks seen for all the milled samples when compared to the as-received material, the PXD analysis (top of Figure 1) also shows an increase of the β-$Ca(BH_4)_2$ content with increased milling time in the case of the $\alpha_{\beta\gamma}$ sample. This indicates that the temperatures achieved in the vials during the milling process are enough to induce a phase transformation from the low temperature α- to the high temperature β-$Ca(BH_4)_2$. The transition temperature is about 167 °C under a helium gas flow and with a heating rate of 5 °C/min [1].

This behavior is in agreement with the fact that β-$Ca(BH_4)_2$ becomes more stable compared to α-$Ca(BH_4)_2$ with increasing temperature [19]. The Differential scanning calorimetry (DSC) curves (bottom of Figure 1) show a small decrease of the decomposition temperature of the samples with milling time, from approximately the 357 °C of the 1 h milled sample to the 353 °C of the 8 h sample, and thus indicates that the β-$Ca(BH_4)_2$ formed during milling is less stable that the same phase formed during heating. This could be related to smaller crystallites in the milling case. No big changes in the polymorphic ratio with milling time are observed in the PXD patterns of the γ sample (Figure 1b), leading to no shift of the decomposition temperatures in the DSC curves (Figure 1d). The lack of change in this case agrees with the gradual and broad temperature range in which the γ to β transformation occurs [31] and the fact that γ-$Ca(BH_4)_2$ is metastable in the whole temperature range below the

decomposition temperature of the high temperature β polymorph [19]. Thus, it seems that under the ball milling conditions used in this work, the γ to β transformation is less probable than the α to β transformation. The behavior is reproducible and indicates that not only the as-received $Ca(BH_4)_2$ polymorphs have different decomposition temperatures [1], but that ball milling effects also depend on the polymorphic composition of the samples.

2.2. Milling Effects on $Ca(BH_4)_2$ with TiF_3

PXD patterns of the samples containing 1.6 and 10 mol% of TiF_3 show that no new species are formed during the milling with $Ca(BH_4)_2$ (Figure 2). In particular, no cation or anion substitutions, such as those found for $NaBH_4$ [24], are observed. In all the cases, $Ca(BH_4)_2$ and TiF_3 in the crystalline form are still present in the milled material. The broadening of the Bragg peaks and the loss of signal to noise ratio of the measurements are an indication of the finer crystallite size introduced by ball milling.

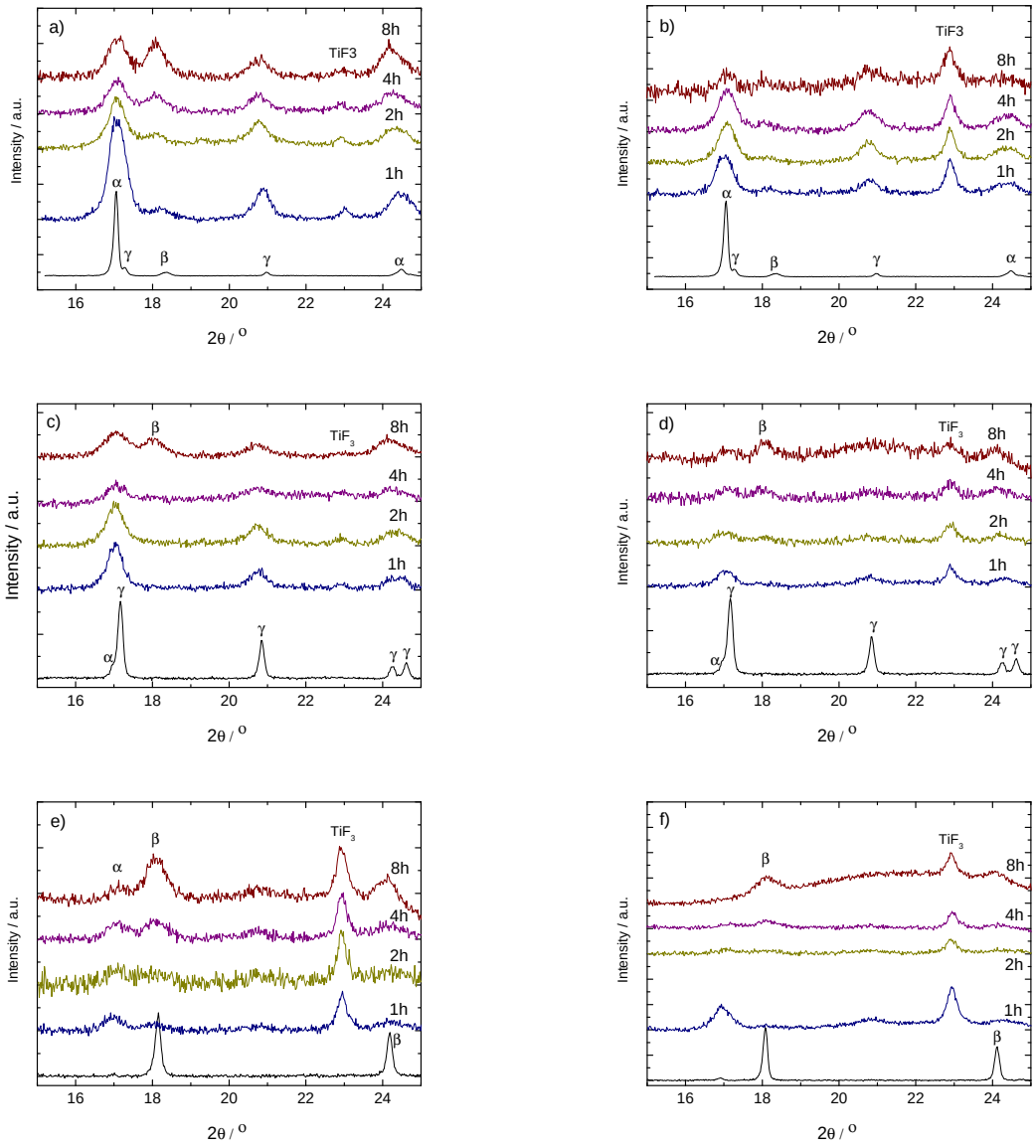

Figure 2. PXD results on ball milled $\alpha_{\beta\gamma}$ (up, (**a**,**b**)) and γ (middle, (**c**,**d**)) with 1.6 mol% (left-hand side, (**a**,**c**)) and 10 mol% (right-hand side, (**b**,**d**)) of TiF_3. Bottom: PXD results on ball milled β_{64} (left-hand side, (**e**)) and β_{92} (right-hand side, (**f**)) with 10 mol% of TiF_3. Samples were taken from the vials after 1, 2, 4 and 8 h milling. The pattern of the as-received sample is included for comparison.

The PXD results are confirmed by IR spectroscopy (Figures 3 and 4), where the only differences between the as-received and the samples with TiF_3 are observed in the 400–1000 cm^{-1} range. In particular, the samples with additive show a prominent feature at approximately 554 cm^{-1}, which increases with additive amount.

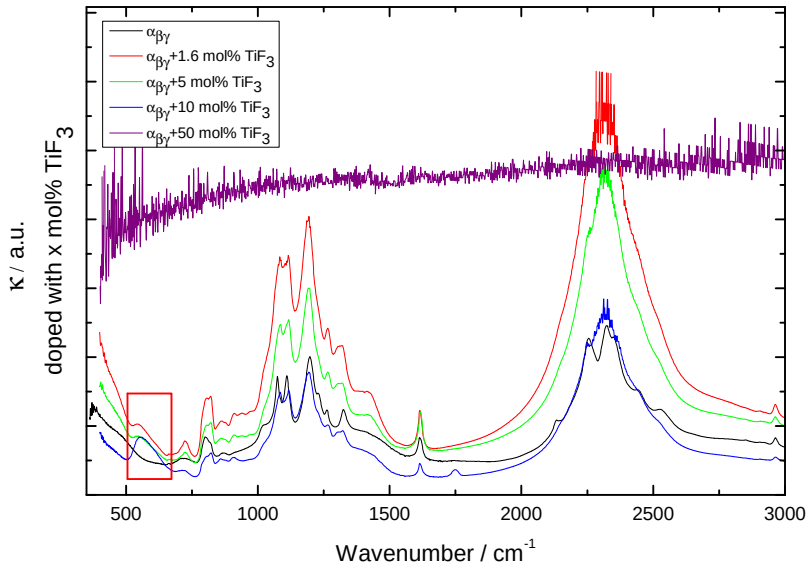

Figure 3. Infrared (IR) spectra for $\alpha_{\beta\gamma}$-$Ca(BH_4)_2$ samples with additive. External modes corresponding to lattice vibrations in TiF_3 are marked with a red box. The spectrum of a sample prepared by milling $\alpha_{\beta\gamma}$ + 50 mol% TiF_3 is also included.

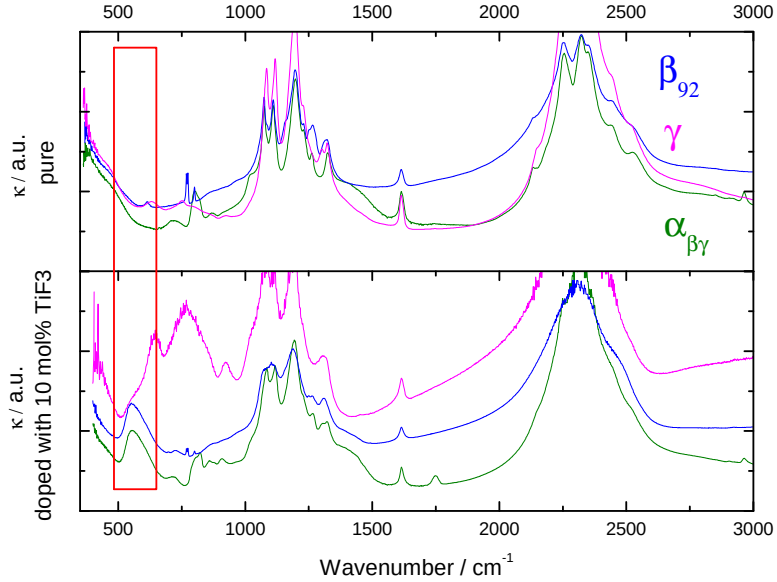

Figure 4. IR spectra for as-received (upper panel) and $\alpha_{\beta\gamma}$-, β_{92} and γ with 10 mol% of TiF_3. External modes corresponding to lattice vibrations in TiF_3 are marked with a red box.

According to symmetry selection rules, the two IR active vibrational modes in borohydrides are the νBH stretching and δHBH bending modes at 2200–2300 cm^{-1} and 1100 cm^{-1}, respectively. Other bands corresponding to overtones and combinations are also seen experimentally [1]. Below 1000 cm^{-1}, external and librational modes between BH_4^- and Ca^{2+} can be distinguished in the IR spectra [1].

The addition of TiF_3 changes the decomposition behavior of the samples after milling compared to the as-received materials. Thus, while α-$Ca(BH_4)_2$ + 1.6 mol% TiF_3 (Figure 2a) transforms into

β-$Ca(BH_4)_2$ with increasing milling time, the addition of 10 mol% of TiF_3 (Figure 2b) seems to have no effect. This indicates that, for small amounts of TiF_3, the α-$Ca(BH_4)_2$ samples are mostly affected by the polymorph nature and the milling process and not by the additive. Increasing the additive content makes the milling conditions harsher for the high temperature polymorph as well as for the original α borohydride, as indicated by the loss of crystallinity of the α polymorph in Figure 2a.

On the other hand, for γ-$Ca(BH_4)_2$ (Figure 2c,d), the addition of TiF_3 in both 1.6 and 10 mol% leads to an increase of the content of the high temperature polymorph β-$Ca(BH_4)_2$ with milling time. This shows that in the γ case, TiF_3 has a more prominent role in improving the kinetic decomposition of the borohydride than for the α polymorph. For β-$Ca(BH_4)_2$ the addition of 10 mol% of TiF_3 has different effects depending on the polymorphic purity of the sample. In the case of β_{64} (Figure 2e), an increase of the α-$Ca(BH_4)_2$ content is induced by the additive, while for β_{92} (Figure 2d), the crystalline borohydride is affected strongly by the milling time, with the disappearance and formation of α- and β-$Ca(BH_4)_2$ at different stages, respectively.

The PXD results strongly correlate with the DSC curves in the decomposition region of the high temperature polymorph β (Figure 5). In some cases, these decomposition curves show more steps than the expected main two peaks corresponding to the formation of an intermediate compound and the subsequent decomposition of the high temperature polymorph [32]. This is due to the presence of mixed-polymorphs in the samples formed during milling and their different transformation and decomposition temperatures [1]. The DSC curves also show that a decrease of the decomposition temperature with increasing milling time takes place in all the cases containing TiF_3. Exceptions are explained by the presence or absence of α-$Ca(BH_4)_2$ in the samples and by the ratio between α- and β-$Ca(BH_4)_2$. In most cases, larger α/β ratios lead to lower decomposition temperatures. This agrees with the results by Llamas-Jansa et al. [1] on pure $Ca(BH_4)_2$ polymorphs and shows the impact of a milling process. From the present results, the sample with the lowest desorption temperature is α-$Ca(BH_4)_2$ + 10 mol% TiF_3, with a temperature shift of approx. 27 °C compared to the as-received material (Figure 6).

Finally, the additive amount was increased to 20 and 50 mol% of TiF_3 (Figure 7). Increasing the amount of TiF_3 led to the formation of CaF_2 and TiO_2 and, therefore, other effects than merely kinetics are introduced in the behavior of the $Ca(BH_4)_2$ samples. The presence of oxygen in $Ca(BH_4)_2$ is expected and is related to contamination during the handling of the materials or as part of the commercial products. The fact that the sample containing 50 mol% of TiF_3 led to CaF_2 and TiO_2 also indicates that the milling conditions were harsh enough to decompose the original $Ca(BH_4)_2$ and TiF_3. This was confirmed by the corresponding DSC curves, that showed a decrease of the decomposition peak for 10 and 20 mol%, but no decomposition peaks in the 50 mol% case (not plotted). The lack of borohydride in this sample was confirmed by IR spectroscopy (as shown in Figure 3).

2.3. Activation Energies

Sample α, containing 98% of the α-$Ca(BH_4)_2$ polymorph (Table 1), was ball milled for 8 h without stop, with and without 10 mol% TiF_3. The milling products were separated in smaller samples and then heated at different heating rates in order to calculate their activation energies from a generalization of the Kissinger equation [33]:

$$ln(\beta/T_{max}^2) = -E_a/RT_{max}, \quad (2)$$

where β is the heating rate and T_{max} is the temperature of the endothermic peak at its maximum; R is the gas constant and E_a is the activation energy. Activation energies calculated from the graphical representation of this equation lead to values of 199 ± 3 and 204 ± 1 $kJmol^{-1}$ for the samples with additive and without additive, respectively (Figure 8). The small difference indicates some success by TiF_3 to destabilize $Ca(BH_4)_2$, in agreement with the observed decomposition behavior.

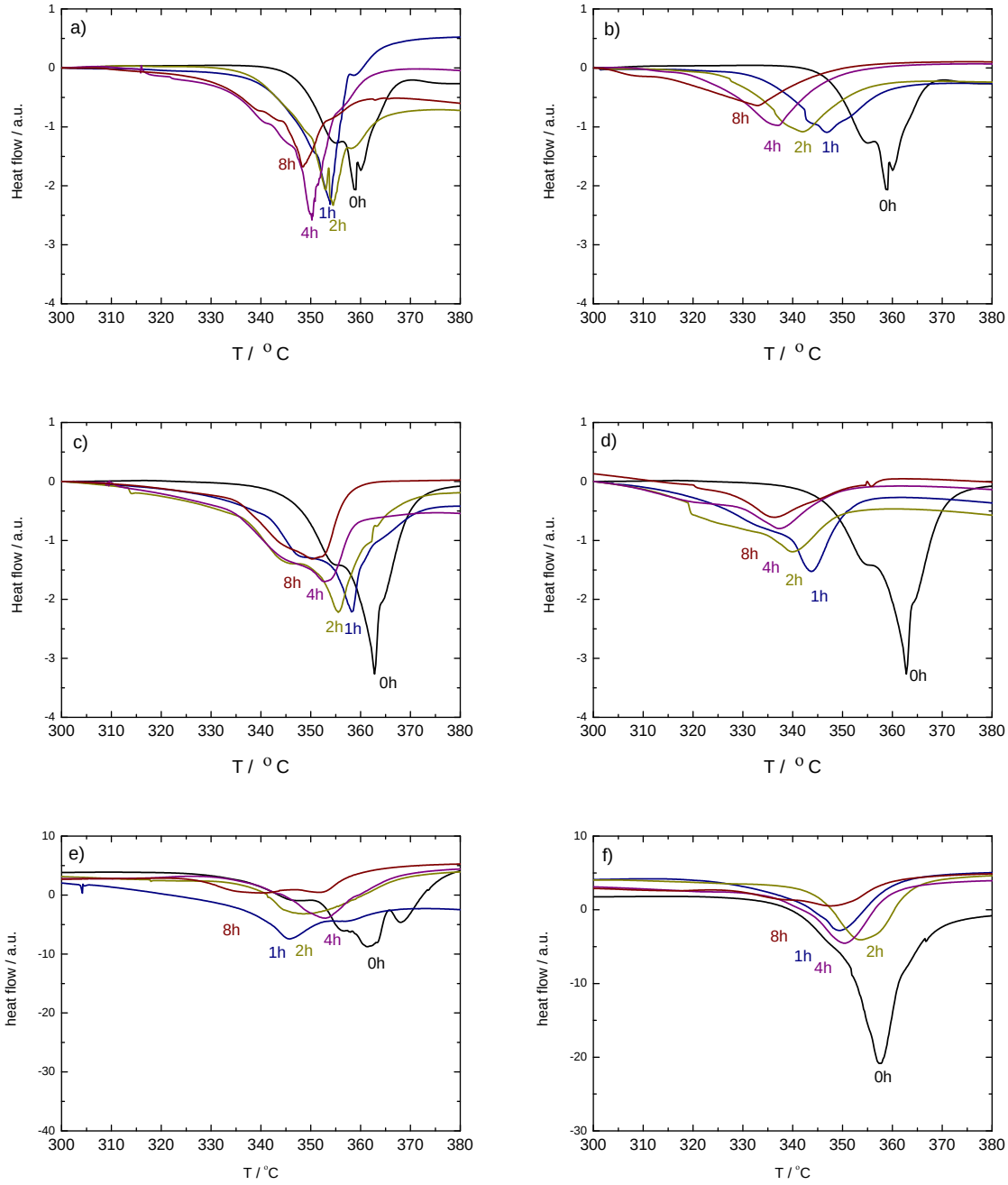

Figure 5. Corresponding DSC curves of ball milled $\alpha_{\beta\gamma}$ (top, (**a**,**b**)) and γ (middle, (**c**,**d**)), with 1.6 mol% (left-hand side, (**a**,**c**)) and 10 mol% (rigth-hand side, (**b**,**d**)) of TiF_3, respectively. Bottom: Corresponding DSC curves of the ball milled β_{64} (left-hand side, (**e**)) and β_{92} (right-hand side, (**f**)) with 10 mol% of TiF_3. Only the main decomposition region between 330 and 380 °C is shown. Measurements were done under dynamic conditions in protective Ar flow, with 2 °C/min heating rates. The curves have been shifted to show the peak trend.

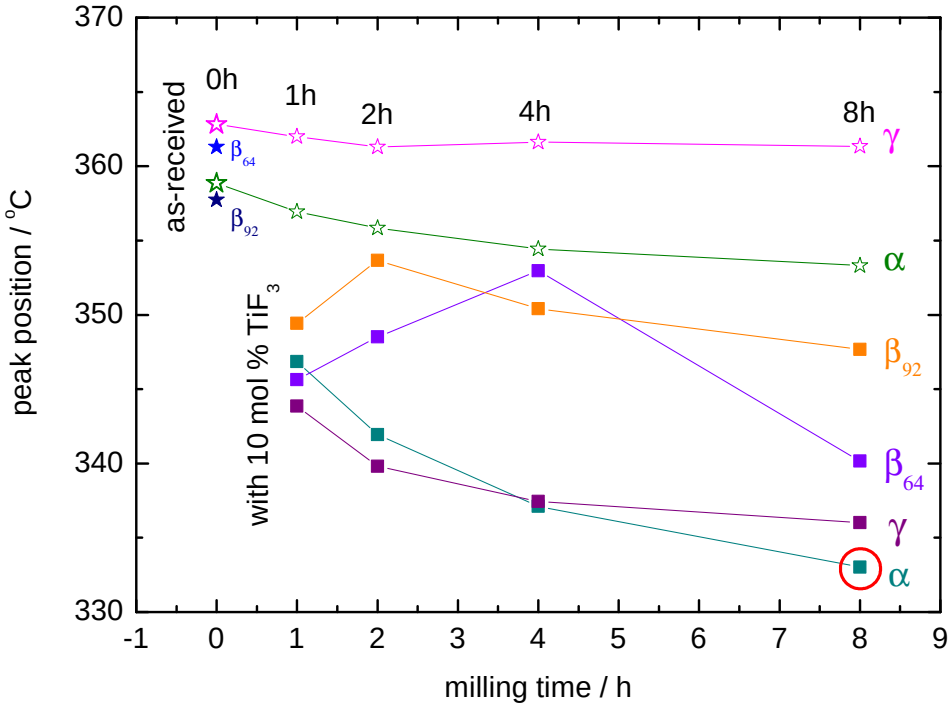

Figure 6. Position of the decomposition peaks as observed by DSC. The lowest decomposition temperature corresponds to $\alpha_{\beta\gamma}$ + 10 mol% TiF_3 milled for 8 h and is marked by a red circle. 0 h means the sample was measured as-received.

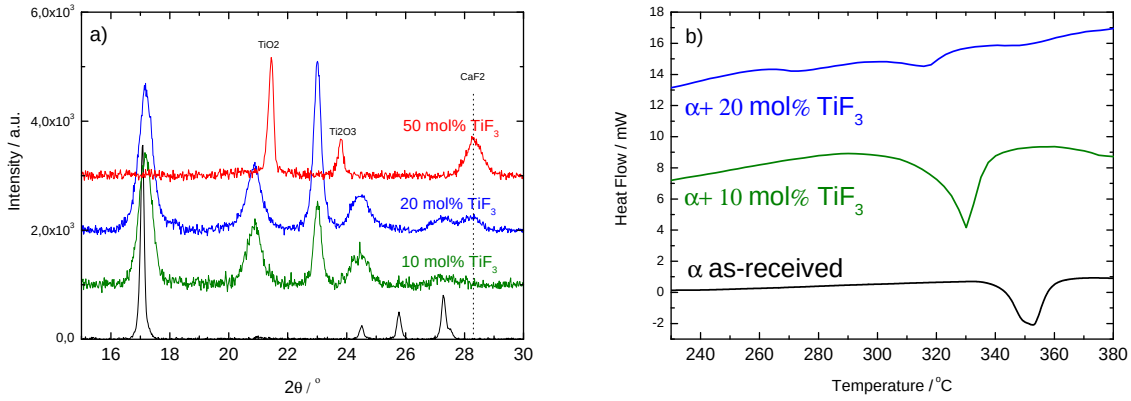

Figure 7. PXD (left-hand panel, (**a**)) and DSC (right-hand panel, (**b**)) results of ball milled α with 10, 20 and 50 mol% of TiF_3 after 8 h continuous milling. The results for the as-received material are included for comparison.

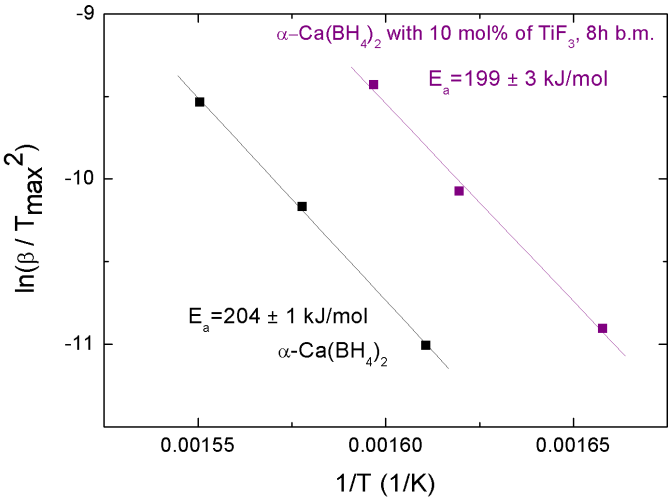

Figure 8. Kissinger plot corresponding to as-received α and α + 10 mol% TiF_3 milled for 8 h.

3. Materials and Methods

The present study was performed on $Ca(BH_4)_2$ samples containing different amounts of the α, β, and γ polymorphs (Table 1). All polymorphs were crystalline and stable at room temperature (RT). Samples $\alpha_{\beta\gamma}$ and α were prepared from commercial $Ca(BH_4)_2$.2THF by heating in vacuum up to 160 °C for 1 h, while γ was synthesized by wet chemistry of CaH_2 + $2Et_3N.BH_3$. The β_{64} and β_{92} samples containing 64 and 92 mol% of β phase, respectively, were synthesized by a solvent-free method based on the reaction of metal hydrides with diborane and subsequent ball milling. The details of the synthesis methods are described elsewhere [8,34–36]. Sample handling was carried out in MBraun Unilab glove boxes filled with purified argon (<1 ppm O_2, H_2O) and transportable glove bags filled with Ar.

Milling with and without additive was carried out in Ar using a Fritsch Pulverisette 7 (P7) planetary mill at 505 rpm. Steel balls 10 mm in diameter and tempered steel vials were used. Small amounts of milled material were extracted from the vials after 1, 2, 4, and 8 h, always keeping the ball-to-powder ratio constant to 50:1. TiF_3 powder (Aldrich, 99%) was added to the different polymorphs in 1.6, 5, 10, 20 and 50 mol% amounts (Table 2). Tests with 5 mol% of ScH_2 and AlF_3 showed little effect on the decomposition temperature of $Ca(BH_4)_2$ and are not discussed here. As shown by Llamas et al. [24], stoichiometric mixtures may lead to new compounds that alter the decomposition path (thermodynamics) of a borohydride. In this study, only kinetic effects were investigated.

Table 1. Sample list. Phase fractions were obtained from PXD patterns using *F2dd* [17], *Pbca* [18] and *P-4* [17] for α-, γ- and β-$Ca(BH_4)_2$, respectively. Other phases, except for CaH_2 and $FeNi_3$ in β_{92}, where not taken into account.

Sample Name	Highest Content Polymorph	Phase Fraction $\alpha/\beta/\gamma$ (mol%)	Synthesis Method
$\alpha_{\beta\gamma}$	α	67/23/10	from $Ca(BH_4)_2$.2THF [a]
α	α	98/–/2	from $Ca(BH_4)_2$.2THF [a]
γ	γ	8/–/92	from CaH_2 + $2Et_3N.BH_3$ [b]
β_{64}	β	–/64/– [d]	reactive milling in B_2H_6 [c]
β_{92}	β	–/92/–	reactive milling in B_2H_6 [c]

[a] Reference [8,34]; [b] Reference [35]; [c] Reference [36]; [d] also containing $Ca_3(BH_4)_3(BO_3)$.

Table 2. Sample preparation conditions.

Sample Name	Highest Content Polymorph	Milling Time / h	TiF_3 Content / mol%
$\alpha_{\beta\gamma}$	α	1, 2, 4, 8	0, 1.6, 5, 10
α	α	8, 24	10, 20, 50
γ	γ	1, 2, 4, 8	0, 1.6, 5, 10
β_{64}	β	1, 2, 4, 8	10
β_{92}	β	1, 2, 4, 8	10

Powder X-ray diffraction (PXD) patterns were collected in transmission mode using CuKα radiation (λ = 1.5418 Å) in a Bruker AXS D8 Advance Diffractometer equipped with a Göbbel mirror and a LynxEye^{TM} 1D strip detector. Diffraction patterns were obtained at RT in rotating boron containing glass capillaries (0.8 mm ϕ) filled and sealed under Ar atmosphere. Data acquisition was restricted to $2\theta = 5 - 80^{\circ}$, with $\Delta 2\theta = 0.02^{\circ}$ and 2 s/step scanning rates. The phase fraction of the different samples was obtained from the PXD patterns using GSAS [37].

Differential scanning calorimetry (DSC) was carried out between RT and 500 °C in Al crucibles with pierced lid using a Setaram Sensys DSC. Additional DSC measurements were carried out in a STA449F3 Jupiter from NETZSCH using corundum (Al_2O_3) crucibles and pierced lids. In both cases measurements were done under dynamic conditions in protective Ar flow with 2 °C/min heating rates. Additional heating rates of 5 and 10 °C/min were used in the STA449F3 Jupiter to determine sample activation energies. Approximately 30 mg of fresh material was used in every case.

Infrared (IR) spectroscopy was carried out in a Bruker IFS 66v spectrometer with a DTGS detector. The samples were embedded in KBr pellets (7 mm ϕ), with a 0.5% mass concentration. The transmission spectra of the KBr pellets were recorded in the 400–8000 cm^{-1} region, with a 4 cm^{-1} resolution. Scattering contribution to the spectra due to the pellets was considered to be negligible at these wavenumbers. Mass absorption coefficients (κ) were calculated from the transmission (T) data as:

$$\kappa = -lnT(A/m), \quad (3)$$

where A is the area of the pellet in cm^2, and m is the mass of the absorbing sample in g [38]. The spectroscopic curves were further normalized to the strongest peak in both the bending and the stretching regions to allow a better visualization of the peak shifts introduced by the different samples. Peak analysis was carried out in Origin 7.5 using Gaussian curves.

4. Conclusions

The hydrogen desorption peak temperature of $Ca(BH_4)_2$ depends strongly on the composition of the coexistent α, β and γ polymorphs, which is determined by the synthesis method. Additional ball milling affects the kinetics of the material and leads to a lowering of the peak temperature, which is more pronounced by increasing the content of the α polymorph in the sample. The kinetic effect is further decreased by the addition of TiF_3 to the sample, that is, TiF_3 increases the hydrogen desorption rate. The improved kinetics by the addition of TiF_3 was observed without significant dissociation of TiF_3 and, therefore, must be related to the reduction of all the crystallite sizes (including those of TiF_3) due to the ball milling process.

Author Contributions: Conceptualization and methodology for this article as well as experimental investigation, validation, formal analysis, data curation, project administration, provision of materials, supervision, visualization and writing of original draft was carried out by I.L.J., O.F., M.F. and E.G.B. provided samples, while A.Z. and B.C.H. reviewed the original manuscript. Overall resources and funding acquisition by B.C.H. All authors have read and agreed to the published version of the manuscript.

Funding: Financial support from the Research Council of Norway, the FLYHY project (contract no. 226943) and the ERA-NET project Hy-CO (grant#0327791) under the FP7 Program in the European Commission are also gratefully acknowledged.

Acknowledgments: The authors acknowledge the contributions of Claus Nielsen at the Chemistry Department of the University of Oslo for IR spectroscopy and the project team at the SNBL Beam Line, ESRF, Grenoble.

Conflicts of Interest: The authors declare no conflict of interest. The funders had no role in the design of the study; in the collection, analyses, or interpretation of data; in the writing of the manuscript, or in the decision to publish the results.

References

1. Llamas-Jansa, I.; Friedrichs, O.; Fichtner, M.; Bardaji, E.G.; Züttel, A.; Hauback, B.C. The Role of $Ca(BH_4)(2)$ Polymorphs. *J. Phys. Chem. C* **2012**, *116*, 13472–13479. [CrossRef]
2. Kim, J.H.; Jin, S.A.; Shim, J.H.; Cho, Y.W. Reversible hydrogen storage in calcium borohydride $Ca(BH_4)(2)$. *Scr. Mater.* **2008**, *58*, 481–483. [CrossRef]
3. Lee, J.Y.; Lee, Y.S.; Suh, J.Y.; Shim, J.H.; Cho, Y.W. Metal halide doped metal borohydrides for hydrogen storage: The case of $Ca(BH_4)(2)$-CaX_2 (X = F, Cl) mixture. *J. Alloys Compd.* **2010**, *506*, 721–727. [CrossRef]
4. Ibikunle, A.A.; Goudy, A.J. Kinetics and modeling study of a $Mg(BH_4)_2/Ca(BH_4)_2$ destabilized system. *Int. J. Hydrog. Energy* **2012**, *37*, 12420–12424. [CrossRef]
5. Ibikunle, A.A.; Sabitu, S.T.; Goudy, A.J. Kinetics and modeling studies of the $CaH_2/LiBH_4$, $MgH_2/LiBH_4$, $Ca(BH_4)_2$ and $Mg(BH_4)_2$ systems. *J. Alloys Compd.* **2013**, *556*, 45–50. [CrossRef]
6. Minella, C.B.; Garroni, S.; Pistidda, C.; Baro, M.D.; Gutfleisch, O.; Klassen, T.; Dornheim, M. Sorption properties and reversibility of Ti(IV) and Nb(V)-fluoride doped-$Ca(BH_4)_2$–MgH_2 system. *J. Alloys Compd.* **2015**, *622*, 989–994. [CrossRef]
7. Hirscher, M.; Yartys, V.A.; Baricco, M.; von Bellosta Colbe, J.; Blanchard, D.; Bowman, R.C.; Broom, D.P.; Buckley, C.E.; Chang, F.; Chen, P.; et al. Materials for hydrogen-based energy storage—Past, recent progress and future outlook. *J. Alloys Compd.* **2020**, *827*, 153548. [CrossRef]
8. Miwa, K.; Aoki, M.; Noritake, T.; Ohba, N.; Nakamori, Y.; Towata, S.i.; Züttel, A.; Orimo, S.I. Thermodynamical stability of calcium borohydride $Ca(BH_4)(2)$. *Phys. Rev. B* **2006**, *74*, 155122. [CrossRef]
9. Nakamori, Y.; Miwa, K.; Ninomiya, A.; Li, H.W.; Ohba, N.; Towata, S.I.; Züttel, A.; Orimo, S.I. Correlation between thermodynamical stabilities of metal borohydrides and cation electronegativites: First-principles calculations and experiments. *Phys. Rev. B* **2006**, *74*, 045126. [CrossRef]
10. Aoki, M.; Miwa, K.; Noritake, T.; Ohba, N.; Matsumoto, M.; Li, H.W.; Nakamori, Y.; Towata, S.; Orimo, S. Structural and dehydriding properties of $Ca(BH_4)(2)$. *Appl. Phys. Mater. Sci. Process.* **2008**, *92*, 601–605. [CrossRef]
11. Noritake, T.; Aoki, M.; Matsumoto, M.; Miwa, K.; Towata, S.; Li, H.-W.; Orimo, S. Crystal structure and charge density analysis of $Ca(BH_4)_2$. *J. Alloys Compd.* **2010**, *491*, 57–62. [CrossRef]
12. Mao, J.; Guo, Z.; Poh, C.K.; Ranjbar, A.; Guo, Y.; Yu, X.; Liu, H. Study on the dehydrogenation kinetics and thermodynamics of $Ca(BH_4)_2$. *J. Alloys Compd.* **2010**, *500*, 200–205. [CrossRef]
13. Rönnebro, E.; Majzoub, E.H. Calcium borohydride for hydrogen storage: catalysis and reversibility. *J. Phys. Chem. B* **2007**, *111*, 12045–12047. [CrossRef] [PubMed]
14. Rongeat, C.; D'Anna, V.; Hagemann, H.; Borgschulte, A.; Züttel, A.; Schultz, L.; Gutfleisch, O. Effect of additives on the synthesis and reversibility of $Ca(BH_4)(2)$. *J. Alloys Compd.* **2010**, *493*, 281–287. [CrossRef]
15. Minella, C.B.; Garroni, S.; Pistidda, C.; Gosalawit-Utke, R.; Barkhordarian, G.; Rongeat, C.; Lindemann, I.; Gutfleisch, O.; Jensen, T.R.; Cerenius, Y.; et al. Effect of Transition Metal Fluorides on the Sorption Properties and Reversible Formation of $Ca(BH_4)(2)$. *J. Phys. Chem. C* **2011**, *115*, 2497–2504. [CrossRef]
16. Riktor, M.D.; Sørby, M.H.; Muller, J.; Bardaji, E.G.; Fichtner, M.; Hauback, B.C. On the rehydrogenation of decomposed $Ca(BH_4)_2$. *J. Alloys Compd.* **2015**, *632*, 800–804. [CrossRef]
17. Filinchuk, Y.; Rönnebro, E.; Chandra, D. Crystal structures and phase transformations in $Ca(BH_4)(2)$. *Acta Mater.* **2009**, *57*, 732–738. [CrossRef]
18. Buchter, F.; Lodziana, Z.; Remhof, A.; Friedrichs, O.; Borgschulte, A.; Mauron, P.; Züttel, A.; Sheptyakov, D.; Barkhordarian, G.; Bormann, R.; et al. Structure of $Ca(BD_4)(2)$ beta-phase from combined neutron and synchrotron X-ray powder diffraction data and density functional calculations *J. Phys. Chem. B* **2008**, *112*, 8042–8048. [CrossRef]
19. Buchter, F.; Lodziana, Z.; Remhof, A.; Friedrichs, O.; Borgschulte, A.; Mauron, P.; Züttel, A.; Sheptyakov, D.; Palatinus, L.; Chlopek, K.; et al. Structure of the orthorhombic gamma-phase and phase transitions of $Ca(BD_4)(2)$. *J. Phys. Chem. C* **2009**, *113*, 17223–17230. [CrossRef]

20. Borgschulte, A.; Gremaud, R.; Züttel, A.; Martelli, P.; Remhof, A.; Ramirez-Cuesta, A.J.; Refson, K.; Bardaji, E.G.; Lohstroh, W.; Fichtner, M.; et al. Experimental evidence of librational vibrations determining the stability of calcium borohydride. *Phys. Rev. B* **2011**, *83*, 024102. [CrossRef]
21. Rongeat, C.; Lindemann, I.; Borgschulte, A.; Schultz, L.; Gutfleisch, O. Effect of the presence of chlorides on the synthesis and decomposition of $Ca(BH_4)(2)$. *Int. J. Hydrog. Energy* **2011**, *36*, 247–253. [CrossRef]
22. Riktor, M.D.; Filinchuk, Y.; Vajeeston, P.; Bardaji, E.G.; Fichtner, M.; Fjellvåg, H.; Sørby, M.H.; Hauback, B.C. The crystal structure of the first borohydride borate, $Ca_3(BD_4)_3(BO_3)$. *J. Mater. Chem.* **2011**, *21*, 7188–7193. [CrossRef]
23. Llamas Jansa, I.; Kalantzopoulos, G.N.; Nordholm, K.; Hauback, B.C. Destabilization of $NaBH_4$ by Transition Metal Fluorides. *Molecules* **2020**, *25*, 780. [CrossRef] [PubMed]
24. Llamas-Jansa, I.; Aliouane, N.; Deledda, S.; Fonneløp, J.E.; Frommen, C.; Humphries, T.; Lieutenant, K.; Sartori, S.; Sørby, M.H.; Hauback, B.C. Chloride substitution induced by mechano-chemical reactions between $NaBH_4$ and transition metal chlorides. *J. Alloys Compd.* **2012**, *530*, 186–192. [CrossRef]
25. Humphries, T.D.; Kalantzopoulos, G.N.; Llamas-Jansa, I.; Olsen, J.E.; Hauback, B.C. Reversible Hydrogenation Studies of $NaBH_4$ Milled with Ni-Containing Additives. *J. Phys. Chem. C* **2013**, *117*, 6060–6065. [CrossRef]
26. Kalantzopoulos, G.N.; Guzik, M.N.; Deledda, S.; Heyn, R.H.; Muller, J.; Hauback, B.C. Destabilization effect of transition metal fluorides on sodium borohydride. *Phys. Chem. Chem. Phys.* **2014**, *16*, 20483–20491. [CrossRef]
27. Zhang, Z.G.; Wang, H.; Liu, J.W.; Zhu, M. Thermal decomposition behaviors of magnesium borohydride doped with metal fluoride additives. *Thermochim. Acta* **2013**, *560*, 82–88. [CrossRef]
28. Saldan, I.; Frommen, C.; Llamas-Jansa, I.; Kalantzopoulos, G.N.; Hino, S.; Arstad, B.; Heyn, R.H.; Zavorotynska, O.; Deledda, S.; Sørby, M.H.; et al. Hydrogen storage properties of γ–$Mg(BH_4)_2$ modified by MoO_3 and TiO_2. *Int. J. Hydrog. Energy* **2015**, *40*, 12286–12293. [CrossRef]
29. Zavorotynska, O.; El-Kharbachi, A.; Deledda, S.; Hauback, B.C. Recent progress in magnesium borohydride $Mg(BH_4)_2$: Fundamentals and applications for energy storage. *Int. J. Hydrog. Energy* **2016**, *41*, 14387–14403. [CrossRef]
30. Shi, B.; Song, Y. Influence of transition metals Fe, Ni, and Nb on dehydrogenation characteristics of $Mg(BH_4)_2$: Electronic structure mechanisms. *Int. J. Hydrog. Energy* **2013**, *38*, 6417–6424. [CrossRef]
31. Nickels, E.A. Structural and Thermogravimetric Studies of Group I and II Borohydrides. Ph.D. Thesis, Sommerville College, Oxford, UK, 2010.
32. Kim, J.H.; Jin, S.A.; Shim, J.H.; Cho, Y.W. Thermal decomposition behavior of calcium borohydride $Ca(BH_4)_2$. *J. Alloys Compd.* **2008**, *461*, L20–L22. [CrossRef]
33. Llopiz, J.; Romero, M.M.; Jerez, A.; Laureiro, Y. Generalization of the Kissinger equation for several kinetic models. *Thermochim. Acta* **1995**, *256*, 205–211. [CrossRef]
34. Riktor, M.D.; Sørby, M.H.; Chlopek, K.; Fichtner, M.; Buchter, F.; Züttel, A.; Hauback, B.C. In situ synchrotron diffraction studies of phase transitions and thermal decomposition of $Mg(BH_4)(2)$ and $Ca(BH_4)(2)$. *J. Mater. Chem.* **2007**, *17*, 4939–4942. [CrossRef]
35. Fichtner, M.; Chlopek, K.; Longhini, M.; Hagemann, H. Vibrational spectra of $Ca(BH_4)(2)$. *J. Phys. Chem. C* **2008**, *112*, 11575–11579. [CrossRef]
36. Friedrichs, O.; Remhof, A.; Borgschulte, A.; Buchter, F.; Orimo, S.I.; Züttel, A. Breaking the passivation-the road to a solvent free borohydride synthesis. *Phys. Chem. Chem. Phys.* **2010**, *12*, 10919–10922. [CrossRef] [PubMed]
37. Larson, A.; Dreele, R. *General Structure Analysis System (GSAS)*; Report Laur 86-748 ed.; Los Alamos National Laboratory: Los Alamos, NM, USA, 2000.
38. Llamas-Jansa, I. Experimental Study of the Optical and Structural Properties of Carbon Nanoparticles. Ph.D. Thesis, Friedrich-Schiller-Universität Jena, Jena, Germany, 2006.